


**Exchange bias effect and Griffiths phase coexistence in the disordered cobaltite  $\text{Gd}_{0.5}\text{Sr}_{0.5}\text{CoO}_{3-\delta}$** I. Fita,<sup>1,\*</sup> I. O. Troyanchuk,<sup>2</sup> T. Zajarniuk,<sup>1</sup> P. Iwanowski,<sup>1</sup> A. Wisniewski,<sup>1</sup> and R. Puzniak<sup>1</sup><sup>1</sup>*Institute of Physics, Polish Academy of Sciences, Aleja Lotnikow 32/46, PL-02668 Warsaw, Poland*<sup>2</sup>*Scientific-Practical Materials Research Centre NAS of Belarus, P. Brovka Street 19, BY-220072 Minsk, Belarus* (Received 7 September 2018; revised manuscript received 10 December 2018; published 28 December 2018)

The exchange bias (EB) effect and an appearance of the Griffiths phase (GP) were found in half-doped cobaltite  $\text{Gd}_{0.5}\text{Sr}_{0.5}\text{CoO}_{3-\delta}$  exhibiting a significant quenched disorder due to the ion size mismatch between Sr and Gd. The disorder weakens the ferromagnetic (FM) interactions between Co ions, leading to low Curie temperature  $T_C = 90$  K and to a highly nonhomogenous magnetic state above  $T_C$ . A clear GP behavior was detected in the temperature range between  $T_C$  and the Griffiths temperature  $T_G = 225$  K. Moreover, this GP demonstrates a unique feature; namely, the appreciable EB effect exists concomitantly within the GP, suggesting coexisting FM and antiferromagnetic nanocluster phases. It was found that the EB exists in  $\text{Gd}_{0.5}\text{Sr}_{0.5}\text{CoO}_{3-\delta}$  for the entire temperature range below  $T_G = 225$  K, in contrast to the limited low-temperature EB observed so far in perovskite cobaltites. The EB has a different nature in the FM cluster phase below  $T_C$  and in the GP in temperature interval  $T_C < T < T_G$ . The cooling field effect on EB was examined in the GP, and the size of FM clusters was determined to be equal to 6.5 nm.

DOI: [10.1103/PhysRevB.98.214445](https://doi.org/10.1103/PhysRevB.98.214445)**I. INTRODUCTION**

Ferromagnetic (FM) perovskite cobaltites  $R_{1-x}M_x\text{CoO}_3$  ( $R$  = rare-earth metal;  $M$  = Ca, Sr, Ba) have attracted much attention because of their unusual physical properties mainly due to the variable spin state of the Co ion [1–5]. Due to strong competition between the crystal-field splitting energy  $\Delta_{\text{CF}}$  and the intra-atomic (Hund) exchange interaction  $J_{\text{ex}}$ , the  $\text{Co}^{3+}$  ion exhibits three alternative spin configurations: the nonmagnetic low-spin (LS) ( $t^6_{2g}e^0_g$ ;  $S = 0$ ), intermediate-spin (IS) ( $t^5_{2g}e^1_g$ ;  $S = 1$ ), and high-spin (HS) ( $t^4_{2g}e^2_g$ ;  $S = 2$ ) states [6]. Different  $\text{Co}^{3+}$  species may coexist in the crystals and a switching between them depends strongly on doping, temperature, and changes in the crystal structure. The mutual dependence between the spin state and lattice favors the phase separation in cobaltites, exhibiting generally a ground state with coexisting FM hole-rich IS regions, spin-glass (SG) regions, and nonmagnetic hole-poor LS regions [7–9]. Such a phase-separated state causes in the FM cluster glassy behavior [9] and leads to an appearance of the exchange bias (EB) effect [10,11], emergent at the interface of coexisting FM and SG nanoscale regions. In the case of this specific EB, based on the intrinsic FM/SG interfaces with the exchange coupling between FM and SG phases, the frozen SG spins play a role of antiferromagnetic (AFM) ones in traditional exchange-biased FM/AFM systems [12]. The EB effect has been found in low doped  $\text{La}_{1-x}\text{Sr}_x\text{CoO}_3$  ( $x < 0.18$ ) [12,13],  $\text{Pr}_{1-x}\text{Sr}_x\text{CoO}_3$  ( $x = 0.2, 0.3$ ) [14], and  $\text{La}_{0.9}\text{Ba}_{0.1}\text{CoO}_3$  [15] cobaltites, where it was ascribed to the pinning effect at the FM/SG interface. The EB was also reported to exist at the FM/ferrimagnetic interface of  $\text{Nd}_{1-x}\text{Sr}_x\text{CoO}_3$  ( $x = 0.2, 0.4$ )

at temperatures below 10 K [16]. It is worth noticing that the EB effect observed in the above cobaltites is small and emerges only at sufficiently low temperatures.

Phase separation is the source of the Griffiths phase (GP) [17] too, which occurs in doped cobaltites. The GP is a specific phase which represents short-range ordered FM clusters embedded in the paramagnetic matrix and shows nonanalytical magnetic behavior in the temperature range  $T_C < T < T_G$ , between the Curie temperature  $T_C$  and the Griffiths temperature  $T_G$ , at which the FM clusters start to nucleate. Namely, the inverse susceptibility  $\chi^{-1}$  shows below  $T_G$  downward deviation from the Curie-Weiss (CW) law, due to the enhanced magnetization from the FM cluster contribution. Quenched disorder in the structure, i.e., the presence of random local lattice distortion due to the dopant ion size mismatch, is believed to be one of the main reasons for formation of the GP in magnetic perovskites [18]. The quenched disorder in  $\text{ABO}_3$  perovskite structure can be evaluated by the cation disorder parameter  $\sigma^2 = \sum x_i r_i^2 - \langle r_A \rangle^2$ , where  $x_i$ ,  $r_i$ , and  $r_A$  are the fractional occupancies, effective ionic radii, and averaged radius of the  $A$ -site cations, respectively. Interestingly, the clear GP was found recently in  $\text{La}_{1-x}\text{Ca}_x\text{CoO}_3$  cobaltites [19], in contrast to the entirely opposite non-Griffiths-like behavior, specifically, the upward deviation in  $\chi^{-1}$  from the CW law, reported in Sr- and Ba-doped ones [20,21]. This difference was explained to arise from the unique dependence of magnetic interactions among  $\text{Co}^{3+}$  ions on the size of the  $M$  dopant in  $\text{La}_{1-x}M_x\text{CoO}_3$  [19]. Namely, the  $\text{Co}^{3+}$  superexchange interactions are AFM in the crystals doped by Sr and Ba but they are FM in the case of doping by Ca. The FM interactions are assumed to originate between the  $\text{Co}^{3+}$  ions with the IS state, while the AFM ones are associated with  $\text{Co}^{3+}$  ions in the HS state, the concentration of which increases in  $\text{La}_{1-x}M_x\text{CoO}_3$  with lattice expansion induced by increase in size of the  $M$  dopant ion [5,22,23].

\*Corresponding author: ifita@ifpan.edu.pl

It appears that the nature of the magnetic state in cobaltites is complicatedly related to delicate lattice changes and local randomness, due to ion size mismatch, and may lead to the simultaneous existence of both AFM and FM nanocluster phases at temperatures above  $T_C$ .

In the present paper, we show that this exceptional situation happens in  $\text{Gd}_{0.5}\text{Sr}_{0.5}\text{CoO}_{3-\delta}$  disordered cobaltite, where the Griffiths phase emerges as result of substitution of the La ion by the smaller Gd ion, extending in wide temperature interval  $T_C < T < T_G$  where  $T_G \sim 2T_C$ . Importantly, the appreciable EB effect exists concomitantly within the GP, suggesting coexistence of FM and AFM phases. This EB is of a distinct nature as compared to the EB observed further below  $T_C = 90$  K, associated with exchange coupling between FM and SG phases. Finally, we found EB to exist in  $\text{Gd}_{0.5}\text{Sr}_{0.5}\text{CoO}_{3-\delta}$  for the entire temperature range below  $T_G = 225$  K, in contrast to the limited low-temperature EB observed so far in cobaltites.

## II. EXPERIMENTAL DETAILS

A polycrystalline  $\text{Gd}_{0.5}\text{Sr}_{0.5}\text{CoO}_{3-\delta}$  sample was prepared by the standard solid-state reaction described in Ref. [24]. A mixture of  $\text{Gd}_2\text{O}_3$ ,  $\text{SrCO}_3$ , and  $\text{Co}_3\text{O}_4$  oxides taken in a stoichiometric ratio was pressed into pellets, sintered at 1473 K for 5 h in air, and then rapidly cooled down to room temperature. The procedure was repeated to produce a homogeneous solid solution. Notice that samples prepared by using a rapid quenching technique exhibit a high degree of A-cation disorder, providing a low FM ordering temperature  $T_C$  [25]. The studied sample was a single phase with the cubic structure and unit-cell parameters  $a = 3.798$  Å and  $V = 54.79$  Å<sup>3</sup>, according to the powder x-ray-diffraction data analyzed in Ref. [24]. The oxygen content in the sample of  $\sim 2.9$  was estimated by thermogravimetric analysis.

The magnetization measurements, such as temperature dependences and hysteresis loops in both field cooling (FC) and zero-field cooling (ZFC) modes, for the temperature range 10–320 K, in magnetic field up to 90 kOe, as well as measurements of ac susceptibility in the temperature range 10–320 K, were performed by using the vibrating sample magnetometer and ac-susceptibility option of the Physical Property Measurement System (PPMS-9T) made by Quantum Design, and by using the Princeton Applied Research (model 4500) vibrating sample magnetometer as well.

## III. RESULTS AND DISCUSSION

Figure 1(a) presents the low-temperature magnetization  $M$  versus  $T$  curves measured in both FC and ZFC regimes. Both the strong gap between ZFC and FC magnetization branches,  $M_{\text{ZFC}}$  and  $M_{\text{FC}}$ , and the maximum in  $M_{\text{ZFC}}$  at temperatures below which the magnetic moments at small field are blocked suggest an appearance of the FM cluster or SG-like behavior. Spontaneous FM ordering is smeared over an interval of about 30 K with average transition temperature  $T_C = 90$  K, determined as the temperature of the minimum in derivative  $dM_{\text{FC}}/dT$ , see upper inset in Fig. 1(a). This behavior is compatible with the highly inhomogeneous FM cluster phase commonly observed in cobaltites [26]; nevertheless, the FM transition appears to be broader in temperature and the  $T_C$  value

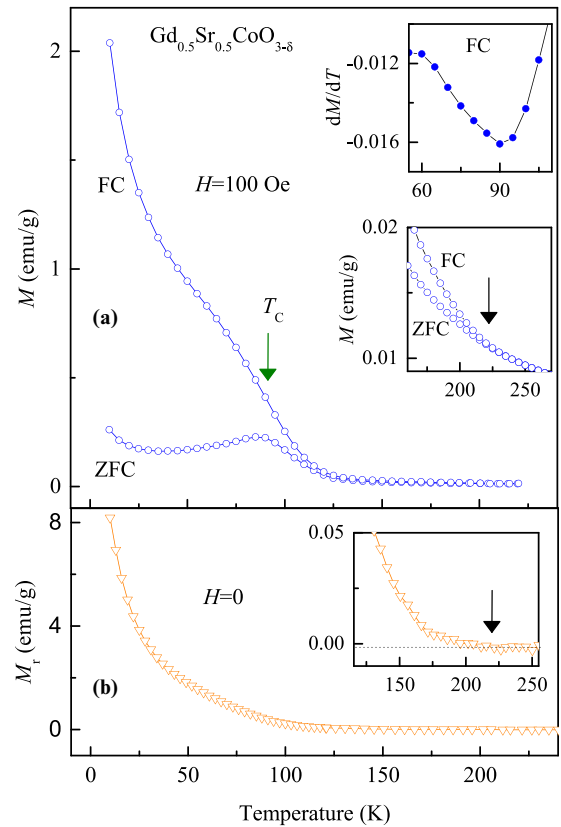


FIG. 1. (a) Temperature dependences of the ZFC and FC magnetization of  $\text{Gd}_{0.5}\text{Sr}_{0.5}\text{CoO}_{3-\delta}$  measured in 100 Oe. The upper inset shows the minimum in derivative  $dM/dT$ , associated with  $T_C$ , and the lower inset shows the onset of divergence in ZFC and FC magnetization. (b) Temperature variation of the remanent magnetization  $M_r$  measured during heating at  $H = 0$ , after field cooling in  $H = 15$  kOe. The inset shows a temperature of disappearance of  $M_r$ .

is lower than that reported in Ref. [27] for  $\text{Gd}_{0.5}\text{Sr}_{0.5}\text{CoO}_3$ . It likely occurs because there are different clusters having unlike Co spin states and  $\text{Co}^{3+}\text{-O-Co}^{4+}$  exchange interactions, due to the local structure deformations in the studied sample with great quenched disorder. Strong increase in  $M_{\text{FC}}$  below 30 K may be explained by paramagnetic CW-like contribution  $M^{\text{Gd}}$  from the weakly interacting large spins ( $S = 7/2$ ) of  $\text{Gd}^{3+}$  ions.

It is shown in the lower inset of Fig. 1(a) that a small gap between ZFC and FC magnetization branches survives at temperatures above  $T_C$  up to the irreversibility temperature of 220 K at which the curves split. In addition, the remanent magnetization  $M_r$ , measured at warming upon zero field immediately after field cooling at  $H = 15$  kOe, disappears at about the same temperature [see Fig. 1(b)]. Both behaviors point to the existence of a small amount of short-range FM phase randomly dispersed in the paramagnetic (PM) matrix. In order to clarify this behavior, we analyzed the inverse susceptibility  $\chi^{-1}$  as a function of temperature, presented in Fig. 2(a), measured between 10 and 320 K in both the ac field of 10 Oe and the dc field of 50 kOe. It was found that the susceptibility thoroughly obeys the CW law  $\chi = C/(T - \theta)$ , with parameters  $\theta = +14$  K and  $C = 0.0229$  emu K/g Oe, at high temperatures, and it deviates downward from the CW

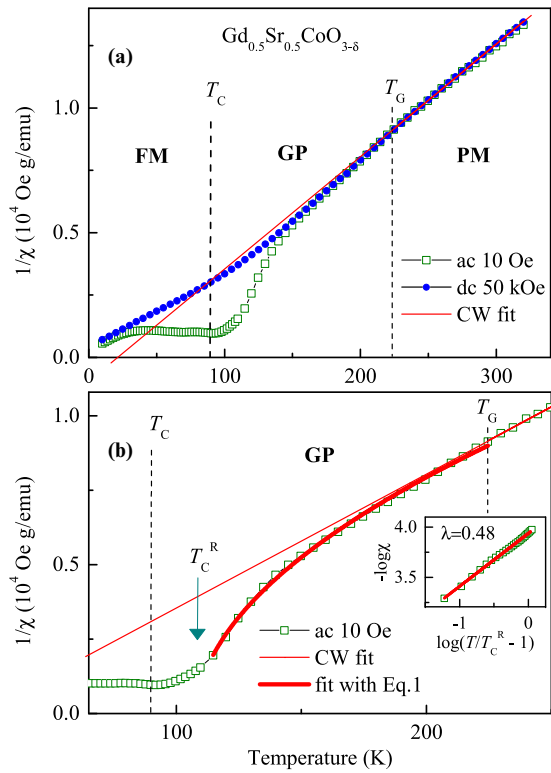


FIG. 2. (a) The inverse susceptibility  $\chi^{-1}$  as function of temperature measured in both the ac field of 10 Oe and the dc field of 50 kOe. The solid line is the CW fit accomplished for the PM state above temperature  $T_G$ . The region of the GP between temperatures  $T_C$  and  $T_G$  is selected. (b) The bold line is the best fit of Eq. (1) to the  $\chi^{-1}(T)$  data with parameters  $T_C^R = 108.3$  K and  $\lambda = 0.48$ . A log-log plot in the inset demonstrates the power-law behavior in  $\chi^{-1}(T)$ .

law below the temperature  $T_G = 225$  K. The small positive value of the Curie-Weiss temperature  $\theta$  suggests competing AFM and FM interactions. Further, the sharp downturn in  $\chi^{-1}$  is observed above the Curie temperature, signifying the appearance of the GP. To identify this behavior as the Griffiths singularity, we examine the  $\chi^{-1}(T)$  curve determined in the ac field of 10 Oe for the power law proposed for the system of FM clusters with distributed sizes embedded in the PM matrix, in the temperature interval  $T_C^R < T < T_G$  [28,29]:

$$\chi^{-1} \propto (T/T_C^R - 1)^{1-\lambda}, \quad (1)$$

where  $T_C^R$  and  $T_G$  are the random and “pure” transition temperatures, respectively, and the exponent  $\lambda$  is positive and lower than unity. The bold line in Fig. 2(b) is the best fit of Eq. (1) to the  $\chi^{-1}(T)$  data for the interval 115–225 K with parameters  $T_C^R = 108.3 \pm 0.8$  K and  $\lambda = 0.48 \pm 0.01$ . A log-log plot in the inset of Fig. 2(b) demonstrates the power-law behavior in  $\chi^{-1}(T)$  which is the hallmark of GP. An analogous fit of Eq. (1) performed in paramagnetic state for temperature interval 225–320 K gives  $\lambda_{\text{PM}} = -0.05 \pm 0.15$  and  $T_{\text{PM}}^R = 0.2 \pm 40$  K, which is close to the value of  $\theta$ , confirming the absence of GP behavior in the PM phase. Thus, the susceptibility behavior in the temperature range between 115 and 225 K unequivocally characterizes the GP. Normally, the applied high magnetic field suppresses the

GP visibility due to an increase in polarization of spins in the PM matrix, masking the FM cluster contribution. It is seen in Fig. 2(a) that the Griffiths state remains visible in  $\text{Gd}_{0.5}\text{Sr}_{0.5}\text{CoO}_{3-\delta}$  at a high enough field of 50 kOe, suggesting the robust FM-cluster-phase contribution to the total magnetization with respect to the PM matrix one. This might point to a complex microscopic structure of the GP, containing both FM and AFM clusters. The presence of AFM clusters in the PM matrix may lead to diminishing its magnetization, as compared to that of the pure PM phase, similarly to the behavior observed in  $\text{La}_{1-x}\text{Sr}_x\text{CoO}_3$  above  $T_C$  [20]. Notably, the GP in  $\text{Gd}_{0.5}\text{Sr}_{0.5}\text{CoO}_{3-\delta}$  is extended for the much wider temperature interval  $\sim 100$  K as compared to that observed in  $\text{La}_{1-x}\text{Ca}_x\text{CoO}_3$  ( $0.1 < x < 0.25$ ) cobaltites, for which both the GP range and exponent  $\lambda$  were found to decrease (this signifies a weakening of the GP) with increasing doping  $x$  [19]. On the other hand, the  $\text{La}_{0.5}\text{Sr}_{0.5}\text{CoO}_3$  exhibits an opposing non-Griffiths-like behavior [20], suggesting the existence of AFM clusters within the PM matrix, in wide temperature interval  $\sim 100$  K above  $T_C$ . Comparing features of different compositions, it can be suggested that the Gd for La substitution introduces a strong quenched disorder in  $\text{Gd}_{0.5}\text{Sr}_{0.5}\text{CoO}_{3-\delta}$ , due to the ion size mismatch between Sr (1.31 Å) and Gd (1.107 Å), leading to a conversion of the non-Griffiths-like phase in  $\text{La}_{0.5}\text{Sr}_{0.5}\text{CoO}_3$  to the pure GP in  $\text{Gd}_{0.5}\text{Sr}_{0.5}\text{CoO}_{3-\delta}$ . Such disorder produces a highly nonhomogeneous state when different values of exchange coupling may be allocated randomly to different sites of the lattice. This likely causes a coexistence of short-range FM and AFM clusters for  $T_C < T < T_G$ . To obtain insight into the nature of the GP, we investigate further both GP and FM clusterlike states below  $T_C$  by magnetization hysteresis loops depending on different field cooling protocols.

Figure 3(a) presents the FC magnetization hysteresis loops of  $\text{Gd}_{0.5}\text{Sr}_{0.5}\text{CoO}_{3-\delta}$  measured with cooling field  $H_{\text{cool}} = 15$  kOe at several temperatures below  $T_C$ . They reveal a substantial EB effect, that is, the FC loop shifts away from the origin, due to the induced EB anisotropy. In contrast, the ZFC hysteresis loop (not shown) is symmetrical, indicating lack of EB. Figure 3(b) demonstrates that EB anisotropy changes sign, namely, the direction of loop shift reverses, when the cooling field alters its sign. The EB field defined as  $H_{\text{EB}} = (H_1 + H_2)/2$  is negative, as typically occurs for applied positive  $H_{\text{cool}}$  [11], while the average coercive field  $H_C = (H_2 - H_1)/2$ , where  $H_1$  and  $H_2$  are the first (negative) and second (positive) coercive fields at the first and second magnetization reversals, respectively, is positive. Excitingly, a clear EB was detected also in the region of the GP, at temperatures  $T_C < T < T_G$ . Figures 3(c) and 3(d) present the FC hysteresis loops at  $T = 100$  and 140 K measured with cooling fields of different polarity, +15 and -15 kOe. The loops indicate a small coercive field and tiny spontaneous magnetization, and they shift from the origin oppositely to the direction of applied  $H_{\text{cool}}$ , representing the negative EB effect [see insets in Figs. 3(c) and 3(d)], whereas the ZFC loops show no EB. Unusually, in the GP locality, both  $H_1$  and  $H_2$  coercive fields appear to be negative at applied positive  $H_{\text{cool}}$ , while they are, as usual, of different sign below  $T_C$ , in the region of the FM cluster state [see Fig. 4(a)]. Moreover, the  $H_1$  and  $H_2$  coercive fields vary nonmonotonically with

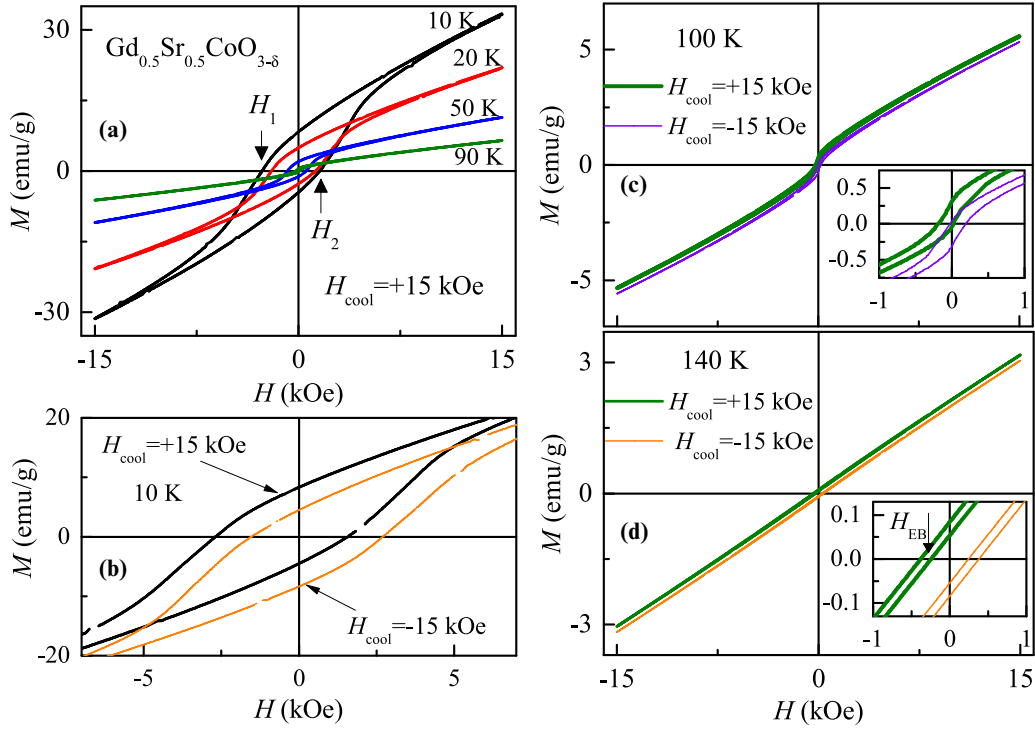


FIG. 3. (a) Magnetization hysteresis loops of  $\text{Gd}_{0.5}\text{Sr}_{0.5}\text{CoO}_{3-\delta}$  measured with cooling field  $H_{\text{cool}} = 15$  kOe at several temperatures below  $T_C$ . Arrows mark the negative  $H_1$  and positive  $H_2$  coercive fields. (b) A reversal of the direction of loop shift with altering the cooling field sign. (c, d) Hysteresis loops at 100 K (c) and at 140 K (d) measured with both  $H_{\text{cool}} = +15$  and  $-15$  kOe. The insets show the loop shifts in the extended scale, and the arrow indicates the EB field  $H_{\text{EB}}$ .

temperature [see inset in Fig. 4(a)], providing a nonmonotonic  $H_{\text{EB}}$  versus  $T$  dependence with the maximum at the midpoint of the GP zone, shown in Fig. 4(b). Such behavior suggests the competition of the factors that are responsible for the EB. Below  $T_C$ , both  $H_{\text{EB}}$  and  $H_C$  fields increase speedily with lowering  $T$ , likely due to the increased anisotropy of the SG phase. The temperature variation of the  $H_{\text{EB}}$  below  $T_C$  was successfully approximated by exponential decay in the form

$$H_{\text{EB}}(T) = H_{\text{EB}}(0) \exp(-T/T_0), \quad (2)$$

where  $H_{\text{EB}}(0)$  is the value of the EB field extrapolated to  $T = 0$  K and  $T_0$  is a constant. The solid line in Fig. 4(b) is the best fit of Eq. (2) to the experimental points with fitted parameters  $H_{\text{EB}}(0) = -785 \pm 40$  Oe and  $T_0 = 27.3 \pm 1.7$  K. The empirical expression (2) is known to describe well  $H_{\text{EB}}(T)$  behavior in various systems with frustrated interactions [30]; therefore, the reasonable approximation obtained above verifies an essential role of the SG phase in the nature of the EB observed at  $T < T_C$ .

The EB effect in  $\text{Gd}_{0.5}\text{Sr}_{0.5}\text{CoO}_{3-\delta}$  can be interpreted within the intuitive Meiklejohn-Bean (MB) model regarding a system of small isolated FM regions (clusters) embedded in the AFM matrix. Within this model the  $H_{\text{EB}}$  is determined by the ratio of the interfacial exchange energy  $J$  to the product of magnetization  $M_{\text{FM}}$  and thickness  $t_{\text{FM}}$  of the FM layers, and depends on both AFM anisotropy  $K_{\text{AFM}}$  and thickness of the AFM layers  $t_{\text{AFM}}$  [31]:

$$H_{\text{EB}} = \begin{cases} (-J/M_{\text{FM}}t_{\text{FM}})(1 - 1/4R^2)^{1/2} & \text{for } R \geq 1 \\ 0 & \text{for } R < 1 \end{cases}, \quad (3)$$

where the parameter  $R \equiv K_{\text{AFM}}t_{\text{AFM}}/J$  determines the region of existing EB in the system; namely, the EB exists only when  $R \geq 1$ , i.e., when the AFM anisotropy energy  $K_{\text{AFM}}t_{\text{AFM}}$  is large enough. In the case of a system comprising the FM clusters of size  $D$ , distributed in an AFM matrix, one needs to replace  $t_{\text{FM}}$  by  $D/6$  and to take into account that the distance between FM clusters plays the role of  $t_{\text{AFM}}$  [11]. For the case of  $\text{Gd}_{0.5}\text{Sr}_{0.5}\text{CoO}_{3-\delta}$ , exhibiting below  $T_C$  the cluster glass state composed of the FM clusters embedded in the SG matrix, Eq. (3) may be adopted for the description of EB, resulting from the exchange interaction at FM/SG interfaces. However, one should take into account the SG anisotropy  $K_{\text{SG}}$  instead of the AFM anisotropy  $K_{\text{AFM}}$  and the distance between FM clusters  $t_{\text{SG}}$  instead of the thickness of the AFM layers  $t_{\text{AFM}}$ . Accordingly, the EB effect may occur in  $\text{Gd}_{0.5}\text{Sr}_{0.5}\text{CoO}_{3-\delta}$  only if the SG anisotropy is strong and the energy  $K_{\text{SG}}t_{\text{SG}}$  is large enough to be capable to pin the FM cluster moments. From this point of view, the strong increase in  $H_{\text{EB}}$  at very low temperatures may be explained by a robust enhancement of the SG anisotropy. The increase in SG anisotropy upon approaching zero temperature is a typical feature of SG, which is verified here by the increase of the coercive field  $H_C$  [see Fig. 4(c)].

On the other hand, to recognize within the MB model the nonmonotonic  $H_{\text{EB}}$  versus  $T$  dependence observed in the GP zone (temperature range  $T_C < T < T_G$ ), we should assume that FM clusters within the GP exhibit a complex structure, consisting of the FM core and magnetically disordered shell showing AFM- or SG-like features. Such magnetic heterostructures alike to the FM nanoparticles are known to



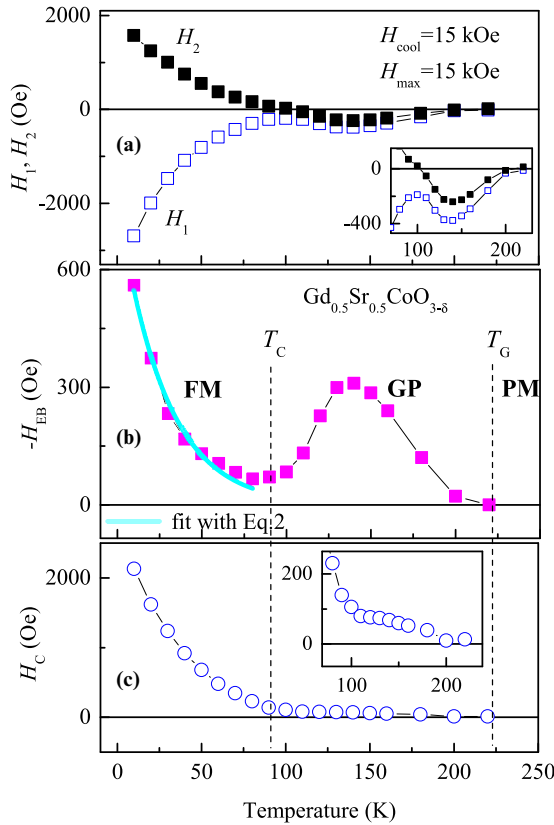


FIG. 4. (a) Variation of coercive fields  $H_1$  and  $H_2$  with temperature for the loops measured with  $H_{cool} = 15$  kOe and  $H_{max} = 15$  kOe. The inset shows nonmonotonic variation of  $H_1$  and  $H_2$  in the region of GP. (b) Nonmonotonic change of  $H_{EB}$  with temperature in the GP, and increase of  $H_{EB}$  with lowering  $T$  in the FM phase. Temperature regions of FM, GP, and PM phases are marked. The solid line shows the fit with Eq. (2). (c) The average coercive field  $H_C$  vs  $T$  dependence.

make available the EB effect [11]; moreover, historically the EB effect was first discovered by Meiklejohn and Bean in isolated Co/CoO nanoparticles with core-shell structure [10]. As seen in Fig. 2, the inverse susceptibility  $\chi^{-1}$  starts to deviate largely below 140 K, i.e. at approaching  $T_C$ , due to the increase in FM magnetization and, hence, due to the increase in FM core size  $D$  or to the increase in concentration of the FM clusters. According to Eq. (3), this may lead to the weakening of EB below 140 K, if the AFM anisotropy of the disordered shell does not change simultaneously and, therefore, becomes incompetent to pin effectively the FM cluster moments. In summary, we conclude that the observed EB effect evidences the coexisting FM and AFM nanocluster phases within the GP at temperatures between  $T_C$  and  $T_G$ . Thus, due to the exceptional quenched disorder, the  $Gd_{0.5}Sr_{0.5}CoO_{3-\delta}$  appears to be situated between  $La_{0.5}Sr_{0.5}CoO_3$ , presenting the non-GP behavior dominated by the AFM clusters, and  $La_{1-x}Ca_xCoO_3$ , exhibiting a clear GP controlled by the FM clusters.

In order to illuminate further the EB in  $Gd_{0.5}Sr_{0.5}CoO_{3-\delta}$  and to distinguish its different nature inside the FM phase region below  $T_C$  and in the GP region above  $T_C$ , we have investigated EB as a function of both cooling field  $H_{cool}$  and maximum field of the loop  $H_{max}$ . Figure 5(a) presents three

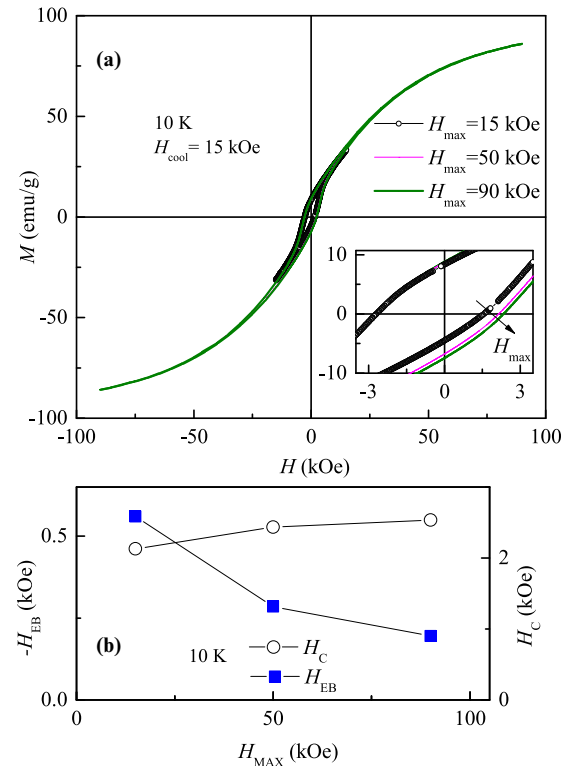


FIG. 5. (a) Three hysteresis loops measured at 10 K with constant cooling field  $H_{cool} = 15$  kOe and different maximum field of the loop  $H_{max}$ . The inset shows the loops in the extended scale. (b) EB field  $H_{EB}$  and coercive field  $H_C$  as a function of the maximum measuring field  $H_{max}$  at constant  $H_{cool} = 15$  kOe and  $T = 10$  K.

hysteresis loops measured at 10 K with constant field  $H_{cool} = 15$  kOe and with different measuring field  $H_{max}$ . The inset shows that with increasing  $H_{max}$  the positive coercive field  $H_2$  increases while the negative field  $H_1$  remains unchanged, hence the EB decreases. It appears that the  $H_{EB}$  field is reduced by a factor of about 3, while the average coercive field  $H_C$  increases by 20%, with increasing  $H_{max}$  from 15 to 90 kOe, as presented in Fig. 5(b).

It should be noted that proper estimation of the EB parameters in strongly anisotropic systems is problematic when the magnetization remains unsaturated even at high magnetic field, and in this case the minor hysteresis loops may exhibit shift, which has nothing in common with the real EB [11]. Nevertheless, it was suggested that the existence of “true” EB in similar systems may be verified by “effectively saturated” hysteresis loops [32,33]. A system is considered to be effectively saturated when the ascending and descending branches of the loop coincide at fields higher than the anisotropy field, i.e., the loops are “closed”. According to Fig. 5(a), the loops at 10 K are closed, namely, the FM component is saturated, within the fields limited by 15 kOe. This implies that the minor loop effect is not a source of an enormous lessening of EB at higher  $H_{max}$ . As an alternative or simultaneous reason, we suggest that a huge contribution to the magnetization from the field-induced polarized spin ( $S = 7/2$ ) array of  $Gd^{3+}$  ions, which may come near to a saturation value of  $3.5 \mu_B/f.u. = 85$  emu/g (calculated for the lattice with half  $Gd^{3+}$  spin in the

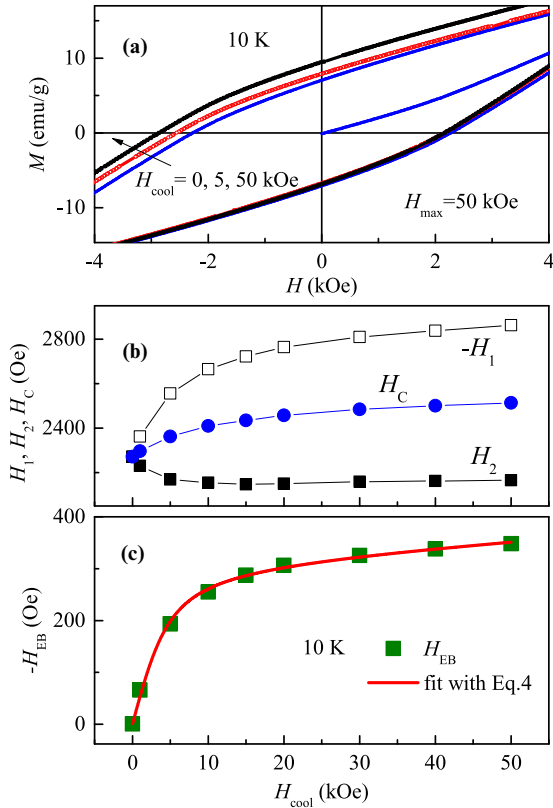


FIG. 6. (a) Enlarged view of hysteresis loops measured at 10 K with constant field  $H_{\text{max}} = 50$  kOe and with different cooling field  $H_{\text{cool}}$ . (b)  $H_{\text{cool}}$  dependences of the first and second,  $H_1$  and  $H_2$ , and average,  $H_C$ , coercive fields. (c)  $H_{\text{EB}}$  vs  $H_{\text{cool}}$  dependence at 10 K. The solid line represents the best fit with Eq. (4).

unit cell), is a realistic cause of suppressed EB at high fields. One can see in Fig. 5(a) that the high-field paramagnetic magnetization of the  $\text{Gd}^{3+}$  spins significantly overcomes the FM contribution from the  $\text{Co}^{3+}$  array, which only attains the value of  $\sim 10$  emu/g. Since this large field-induced  $\text{Gd}^{3+}$  magnetic moment emerges within both interacting FM and SG phases, it effectively reduces magnetic difference between them, leading consequently to a partial suppression of the EB anisotropy induced before by smaller cooling field of 15 kOe. In contrast, the impact of the paramagnetic  $\text{Gd}^{3+}$  moment on EB was found practically insignificant in the GP region, at temperatures  $T_C < T < T_G$ , where the  $M(H)$  loops are surely closed within the field range of 15 kOe [see Figs. 3(c) and 3(d)].

Figure 6(a) presents, in an extended scale, three hysteresis loops measured at 10 K with constant field  $H_{\text{max}} = 50$  kOe and with different cooling field  $H_{\text{cool}}$ . It appears that with increasing  $H_{\text{cool}}$  the EB develops mainly due to the shift of the descending branch of the loop, i.e., the field  $H_1$  increases while  $H_2$  changes only weakly. It is opposite to the changes in loop that occur with increasing  $H_{\text{max}}$  at constant value of  $H_{\text{cool}}$  [see inset in Fig. 5(a)]. Both  $H_{\text{EB}}$  and  $H_C$  fields increase monotonically with increasing  $H_{\text{cool}}$  up to 50 kOe, at constant  $H_{\text{max}} = 50$  kOe, shown in Figs. 6(b) and 6(c). Using the  $H_{\text{EB}}$  versus  $H_{\text{cool}}$  dependence, an estimation of the average size of the FM clusters may be obtained within the model

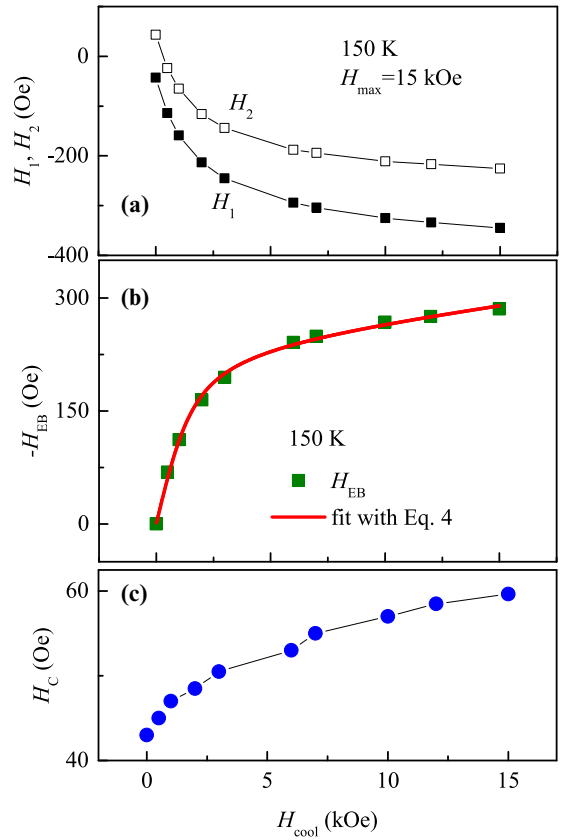


FIG. 7. (a) Variation of the first and second coercive fields,  $H_1$  and  $H_2$ , with cooling field  $H_{\text{cool}}$  at 150 K. (b)  $H_{\text{EB}}$  vs  $H_{\text{cool}}$  dependence at 150 K. The solid line represents the best fit with Eq. (4). (c)  $H_C$  vs  $H_{\text{cool}}$  dependence at 150 K.

proposed in Ref. [34] for phase-separated systems consisting of single-domain FM clusters embedded in the AFM matrix:

$$H_{\text{EB}} \propto J[(J\mu_0/(g\mu_B)^2)L(\mu H_{\text{cool}}/k_B T_f) + H_{\text{cool}}], \quad (4)$$

where  $J$  is the interface exchange constant,  $g = 2$  is the gyromagnetic factor,  $\mu_B$  is the Bohr magneton,  $L$  denotes the Langevin function,  $\mu_0 = 2\mu_B$  is the magnetic moment per  $\text{Co}^{3+}$  ion with spin  $S = 1$ ,  $\mu = N\mu_0$  is the magnetic moment of the FM clusters with  $N$  number of spins within the cluster, and  $T_f = 225$  K is the freezing temperature below which both coercivity and EB appear in  $\text{Gd}_{0.5}\text{Sr}_{0.5}\text{CoO}_{3-\delta}$ . Equation (4) has been successfully used for evaluation of the FM cluster size in a variety of exchange-biased manganites and cobaltites [35]. The solid line in Fig. 6(c) represents the best fit with Eq. (4) obtained for the values of fitting parameters  $N = 850 \pm 80$  and  $J = 40 \pm 12$  K. Exploiting the obtained value of  $N$ , the FM cluster size  $D \approx 4.5$  nm was calculated. However, it was found that the fitting parameter values depend crucially on the loop conditions, similar to the  $H_{\text{EB}}$  field, due to the huge magnetic background of  $\text{Gd}^{3+}$  spins at low temperatures, described above. For illustration, analogous fit to an extra  $H_{\text{EB}}$  versus  $H_{\text{cool}}$  dependence at 10 K, which was expanded up to  $H_{\text{cool}} = 90$  kOe and obtained with loop measuring field  $H_{\text{max}} = 90$  kOe [not shown], gives the cluster size  $D$  of 3.7 nm and the four times larger parameter  $J$  as compared to the former fit. Therefore, we conclude that the model that

leads to Eq. (4) is inapplicable for  $\text{Gd}_{0.5}\text{Sr}_{0.5}\text{CoO}_{3-\delta}$  at low temperatures. In contrast, it is relevant at higher  $T$  when the  $\text{Gd}^{3+}$  spin contribution to the magnetization is small. Figure 7 presents the  $H_{\text{cool}}$  dependences of both coercive fields  $H_1$  and  $H_2$  [Fig. 7(a)],  $H_{\text{EB}}$  [Fig. 7(b)], and  $H_C$  [Fig. 7(c)], derived from the loops taken at 150 K with  $H_{\text{max}} = 15$  kOe. The solid line in Fig. 7(b) is the best fit with Eq. (4), obtained for the values of fitting parameters  $N = 2550 \pm 180$  and  $J = 8.1 \pm 1.6$  K. Using the obtained value of  $N$  and the value of unit-cell volume  $V_{\text{f.u.}} = 54.79 \text{ \AA}^3$ , the FM cluster size  $D \approx 6.5$  nm is estimated. One can estimate the density of FM clusters  $n$  considering the spontaneous magnetization  $M_S = nN\mu_0$ . Taking  $M_S = 0.015 \text{ emu/g} = 6.1 \times 10^{-4} \mu_B/\text{f.u.}$  at 150 K, determined from the ZFC loop, the density of FM clusters of  $n \approx 1.2 \times 10^{-7} \text{ f.u.}^{-1}$  is projected.

#### IV. CONCLUSIONS

In summary, we found coexisting exchange bias effect and Griffiths phase in a wide temperature interval between

$T_C = 90$  K and the Griffiths temperature  $T_G = 225$  K in  $\text{Gd}_{0.5}\text{Sr}_{0.5}\text{CoO}_{3-\delta}$  disordered cobaltite. It appears that total substitution of La ions in  $\text{La}_{0.5}\text{Sr}_{0.5}\text{CoO}_3$  by smaller Gd ions induces a significant quenched disorder in  $\text{Gd}_{0.5}\text{Sr}_{0.5}\text{CoO}_{3-\delta}$ , which leads to the weakening of FM Co–Co interactions and emerging of the GP instead of the non-GP behavior observed above  $T_C$  formerly in  $\text{La}_{0.5}\text{Sr}_{0.5}\text{CoO}_3$  [20]. More interestingly, this GP demonstrates a unique feature; namely, the EB effect exists concomitantly within the GP, suggesting coexisting FM and AFM nanocluster phases. It was found that the EB exists in  $\text{Gd}_{0.5}\text{Sr}_{0.5}\text{CoO}_{3-\delta}$  for the entire temperature range below  $T_G = 225$  K, in contrast to the limited low-temperature EB observed so far in perovskite cobaltites.

#### ACKNOWLEDGMENTS

This work was partially supported by the Polish National Science Centre Grant No. 2014/15/B/ST3/03898 and by the European Union, within the European Regional Development Fund, through the Innovative Economy Grant No. POIG.01.01.02-00-108/09.

- 
- [1] M. A. Señarís-Rodríguez and J. B. Goodenough, *J. Solid State Chem.* **116**, 224 (1995).
- [2] I. O. Troyanchuk, N. V. Kasper, D. D. Khalyavin, H. Szymczak, R. Szymczak, and M. Baran, *Phys. Rev. Lett.* **80**, 3380 (1998).
- [3] P. G. Radaelli and S.-W. Cheong, *Phys. Rev. B* **66**, 094408 (2002).
- [4] M. Kriener, C. Zobel, A. Reichl, J. Baier, M. Cwik, K. Berggold, H. Kierspel, O. Zabara, A. Freimuth, and T. Lorenz, *Phys. Rev. B* **69**, 094417 (2004).
- [5] D. Phelan, Despina Louca, K. Kamazawa, M. F. Hundley, and K. Yamada, *Phys. Rev. B* **76**, 104111 (2007).
- [6] M. A. Korotin, S. Yu. Ezhov, I. V. Solovyev, V. I. Anisimov, D. I. Khomskii, and G. A. Sawatzky, *Phys. Rev. B* **54**, 5309 (1996).
- [7] P. L. Kuhns, M. J. R. Hoch, W. G. Moulton, A. P. Reyes, J. Wu, and C. Leighton, *Phys. Rev. Lett.* **91**, 127202 (2003).
- [8] M. J. R. Hoch, P. L. Kuhns, W. G. Moulton, A. P. Reyes, J. Lu, J. Wu, and C. Leighton, *Phys. Rev. B* **70**, 174443 (2004).
- [9] D. N. H. Nam, K. Jonason, P. Nordblad, N. V. Khiem, and N. X. Phuc, *Phys. Rev. B* **59**, 4189 (1999).
- [10] W. H. Meiklejohn and C. P. Bean, *Phys. Rev.* **102**, 1413 (1956); **105**, 904 (1957).
- [11] J. Noguees, J. Sort, V. Langlais, V. Skumryev, S. Surinach, J. S. Munoz, and M. D. Baro, *Phys. Rep.* **422**, 65 (2005).
- [12] Y. K. Tang, Y. Sun, and Z. H. Cheng, *Phys. Rev. B* **73**, 174419 (2006).
- [13] W. G. Huang, X. Q. Zhang, H. F. Du, R. F. Yang, Y. K. Tang, Y. Sun, and Z. H. Cheng, *J. Phys.: Condens. Matter* **20**, 445209 (2008).
- [14] M. Patra, S. Majumdar, and S. Giri, *J. Appl. Phys.* **107**, 033912 (2010).
- [15] I. Fita, R. Puzniak, A. Wisniewski, V. Markovich, I. O. Troyanchuk, and Yu. G. Pashkevich, *J. Appl. Phys.* **114**, 153910 (2013).
- [16] M. Patra, M. Thakur, S. Majumdar, and S. Giri, *J. Phys.: Condens. Matter* **21**, 236004 (2009).
- [17] R. B. Griffiths, *Phys. Rev. Lett.* **23**, 17 (1969).
- [18] J. Deisenhofer, D. Braak, H.-A. Krug von Nidda, J. Hemberger, R. M. Eremina, V. A. Ivashin, A. M. Balbashov, G. Jug, A. Loidl, T. Kimura, and Y. Tokura, *Phys. Rev. Lett.* **95**, 257202 (2005).
- [19] S. M. Zhou, Y. Li, Y. Q. Guo, J. Y. Zhao, X. Cai, and L. Shi, *J. Appl. Phys.* **114**, 163903 (2013).
- [20] C. He, M. A. Torija, J. Wu, J. W. Lynn, H. Zheng, J. F. Mitchell, and C. Leighton, *Phys. Rev. B* **76**, 014401 (2007).
- [21] W. G. Huang, X. Q. Zhang, G. K. Li, Y. Sun, Q. A. Li, and Z. H. Cheng, *Chin. Phys. B* **18**, 5034 (2009).
- [22] I. O. Troyanchuk, M. V. Bushinsky, and L. S. Lobanovsky, *J. Appl. Phys.* **114**, 213910 (2013).
- [23] J. Yu, Despina Louca, D. Phelan, K. Tomiyasu, K. Horigane, and K. Yamada, *Phys. Rev. B* **80**, 052402 (2009).
- [24] I. O. Troyanchuk, N. V. Kasper, D. D. Khalyavin, A. N. Chobot, G. M. Chobot, and H. Szymczak, *J. Phys.: Condens. Matter* **10**, 6381 (1998).
- [25] V. A. Dudnikov, Yu. S. Orlov, S. Yu. Gavrilkin, M. V. Gorev, S. N. Vereshchagin, L. A. Solovyov, N. S. Perov, and S. G. Ovchinnikov, *J. Phys. Chem. C* **120**, 13443 (2016).
- [26] J. Wu and C. Leighton, *Phys. Rev. B* **67**, 174408 (2003).
- [27] P. V. Vanitha, Anthony Arulraj, P. N. Santhosh, and C. N. R. Rao, *Chem. Mater.* **12**, 1666 (2000).
- [28] A. J. Bray, *Phys. Rev. Lett.* **59**, 586 (1987).
- [29] M. B. Salamon, P. Lin, and S. H. Chun, *Phys. Rev. Lett.* **88**, 197203 (2002).

- [30] N. Moutis, C. Christides, I. Panagiotopoulos, and D. Niarchos, *Phys. Rev. B* **64**, 094429 (2001).
- [31] F. Radu and H. Zabel, in *Magnetic Heterostructures: Advances and Perspectives in Spinstructures and Spintransport*, Springer Tracts in Modern Physics Vol. 227, edited by H. Zabel and S. D. Bader (Springer-Verlag, Berlin, 2008), pp. 97–184.
- [32] J. Geshev, *J. Appl. Phys.* **105**, 066108 (2009).
- [33] J. Geshev, *J. Phys.: Condens. Matter* **21**, 078001 (2009).
- [34] D. Niebieskikwiat and M. B. Salamon, *Phys. Rev. B* **72**, 174422 (2005).
- [35] S. Giri, M. Patra, and S. Majumdar, *J. Phys.: Condens. Matter* **23**, 073201 (2011).